Geol. Mag. **148** (*4*), *2011, pp. 655–669. © Cambridge University Press 2011*
doi:10.1017/S0016756811000124

Authigenesis of native sulphur and dolomite in a lacustrine evaporitic setting (Hellín basin, Late Miocene, SE Spain)

J. LINDTKE*, S. B. ZIEGENBALG*, B. BRUNNER‡, J. M. ROUCHY§, C. PIERRE¶ & J. PECKMANN‖†

*MARUM, Universität Bremen, 28359 Bremen, Germany
‡Max-Planck-Institut für Marine Mikrobiologie, 28359 Bremen, Germany
§Département Histoire de la Terre, Muséum National d'Histoire Naturelle, 75005 Paris, France
¶CNRS-UMR 7159, LOCEAN, Univ. P. and M. Curie, 75252 Paris Cedex 05, France
‖Department für Geodynamik und Sedimentologie, Erdwissenschaftliches Zentrum, Universität Wien, Althanstraße 14, 1090 Wien, Austria

(*Received* 26 July 2010; *accepted* 15 December 2010; *first published online* 17 February 2011)

Abstract – Abundant sulphur is present in the Late Miocene evaporitic sequence of the lacustrine Hellín basin in SE Spain. Weathering of Triassic evaporites controlled the chemical composition of the Miocene lake. The lacustrine deposits comprise gypsum, marlstones, diatomites and carbonate beds. Sulphur-bearing carbonate deposits predominantly consist of early diagenetic dolomite. Abundant dolomite crystals with a spheroidal habit are in accordance with an early formation and point to a microbial origin. The carbon isotopic composition of the dolomite ($\delta^{13}C$ values between −10 and −4 ‰) indicates mixing of lake water carbonate and carbonate derived from the remineralization of organic matter by heterotrophic bacteria. Dolomite precipitated syngenetically under evaporitic conditions as indicated by high oxygen isotope values ($\delta^{18}O$ between +6 and +11 ‰). Nodules of native sulphur are found in gypsum, carbonate beds and marlstone layers. Sulphur formed in the course of microbial sulphate reduction, as reflected by its strong depletion in ^{34}S ($\delta^{34}S$ values as low as −17 ‰). Near to the surface many of the sulphur nodules were in part or completely substituted by secondary gypsum, which still reflects the sulphur isotopic composition of native sulphur (−18 to −10 ‰). This study exemplifies the role of bacterial sulphate reduction in the formation of dolomite and native sulphur in a semi-enclosed lacustrine basin during Late Miocene time.

Keywords: native sulphur, authigenic dolomite, bacterial sulphate reduction, lacustrine setting.

1. Introduction

Native sulphur occurrences are commonly closely associated with evaporites and authigenic carbonates (e.g. Dessau, Jensen & Nakai, 1962; Davis & Kirkland, 1979; Pierre & Rouchy, 1988; Youssef, 1989). Examples of this paragenesis are found in cap rocks of salt diapirs (Ruckmick, Wimberly & Edwards, 1979) and strata-bound deposits like those of northern Iraq (Jassim, Raiswell & Bottrell, 1999), the Delaware basin (Hentz & Henry, 1989), the Carpathian foredeep (Böttcher & Parafiniuk, 1998) and the Mediterranean area (Dessau, Jensen & Nakai, 1962; Anadón, Rosell & Talbot, 1992; Rouchy *et al*. 1998; Ortí, Rosell & Anadón, 2003; Ziegenbalg *et al*. 2010). Both native sulphur and associated authigenic carbonate minerals are commonly considered as products of bacterial sulphate reduction (Feely & Kulp, 1957; Dessau, Jensen & Nakai, 1962; Davis & Kirkland, 1979; Peckmann, Paul & Thiel, 1999; Ziegenbalg *et al*. 2010). In this process, the heterotrophic bacteria oxidize locally abundant crude oil, methane or more pristine organic matter and produce sulphide ions, facilitating subsequent biological or abiological sulphide oxidation to native sulphur (Machel, 1992). Another common consequence of bacterial sulphate reduction is an increase in alkalinity, which results in the precipitation of carbonate minerals (Castanier, Le Métayer-Levrel & Perthuisot, 1999).

Depending on the time of formation of authigenic minerals, Ruckmick, Wimberly & Edwards (1979) distinguished between syngenetic and epigenetic processes. Syngenesis takes place during sedimentation and early diagenesis. Notably, precipitation of carbonate minerals induced by sulphate-reducing bacteria has been described in modern hypersaline environments as well as in laboratory experiments (Lalou, 1957; Vasconcelos & McKenzie, 1997; van Lith *et al*. 2003; Wright & Wacey, 2005). Epigenesis, on the other hand, takes place after deposition during late diagenesis. In the case of epigenetic mineral formation, sulphate, the electron acceptor for the involved heterotrophic bacteria, is delivered by dissolution of sulphate minerals by meteoric waters.

Because bacterial sulphate reduction is dependent on a high supply of sulphate ions, it is favoured in marine rather than in lacustrine environments. In lacustrine settings, methanogenesis tends to act as the main process of organic matter remineralization (Cerling, Bowman & O'Neil, 1988; Talbot & Kelts, 1990). Nevertheless, some examples of carbonate mineral formation induced by sulphate reduction in

†Author for correspondence: joern.peckmann@univie.ac.at

lacustrine deposits are known, including lakes in SW Australia (Wright, 1999) and the eastern USA (Riccioni, Brock & Schreiber, 1996). Sulphur-bearing authigenic carbonates have been reported from the lacustrine Teruel basin in Spain (Anadón, Rosell & Talbot, 1992), where weathering of Triassic marine evaporites provided the sulphate for bacterial sulphate reduction (Utrilla *et al*. 1992). A similar occurrence of native sulphur and associated authigenic carbonates is known from the Late Miocene Hellín basin in SE Spain (Servant-Vildary *et al*. 1990). This restricted basin was typified by lacustrine conditions with only episodic inflow of marine waters (Servant-Vildary *et al*. 1990). Although dolomite and native sulphur have been suggested to derive from bacterial sulphate reduction using sulphate that originated from the dissolution of Triassic gypsum (Servant-Vildary *et al*. 1990), these authigenic minerals have not been studied in detail to date.

Here we present a petrographic and isotopic study on the evaporitic sedimentary sequence of the Hellín basin, focusing on authigenic carbonates and native sulphur. Our study confirms that sulphate-reducing bacteria can be major players in the early diagenesis of lacustrine settings as well, provided that sufficient sulphate ions are available.

2. Geological setting and material

The Hellín basin of SE Spain is an intramontane basin in the external part of the Betic Chain (Fig. 1a). Cretaceous limestones and Triassic evaporites represent the basement of the basin (Servant-Vildary *et al*. 1990). Basin development is attributed to subsidence related to a system of transform faults of an extensional regime, which was active during the Neogene; subsidence terminated in the Late Tortonian (Giese *et al*. 1982; Sanz de Galdeano, 1990; Krijgsman *et al*. 2000; Jolivet *et al*. 2006). Initially the basin was filled by marine sediments dominated by marls and marly carbonate beds. The last marine sedimentation occurred in the Middle Tortonian (Calvo *et al*. 1978). A late phase of N–S-oriented compression started in the Tortonian and led to regional uplift of the crust (Rouchy *et al*. 1998; Jolivet *et al*. 2006). Subsequently, folding of Mesozoic to Cenozoic rocks ended in the development of several local swells that divided the Hellín basin into several sub-basins (Fig. 1b). Formation of a swell to the south close to Calasparra led to the successive isolation of the Hellín basin from the marine environment (Calvo & Elizaga, 1989; Servant-Vildary *et al*. 1990). The change to lacustrine conditions resulted in the accumulation of evaporites and carbonate deposits of the Las Minas de Hellín Formation, which are overlain by carbonate deposits, marls and diatomites (Servant-Vildary *et al*. 1990). The evaporites, mainly represented by gypsum, derived from the dissolution of Triassic evaporites; continued dissolution of gypsum of the Triassic basement (Garcia Domingo *et al*. 1980) is reflected by karst phenomena in the Hellín basin

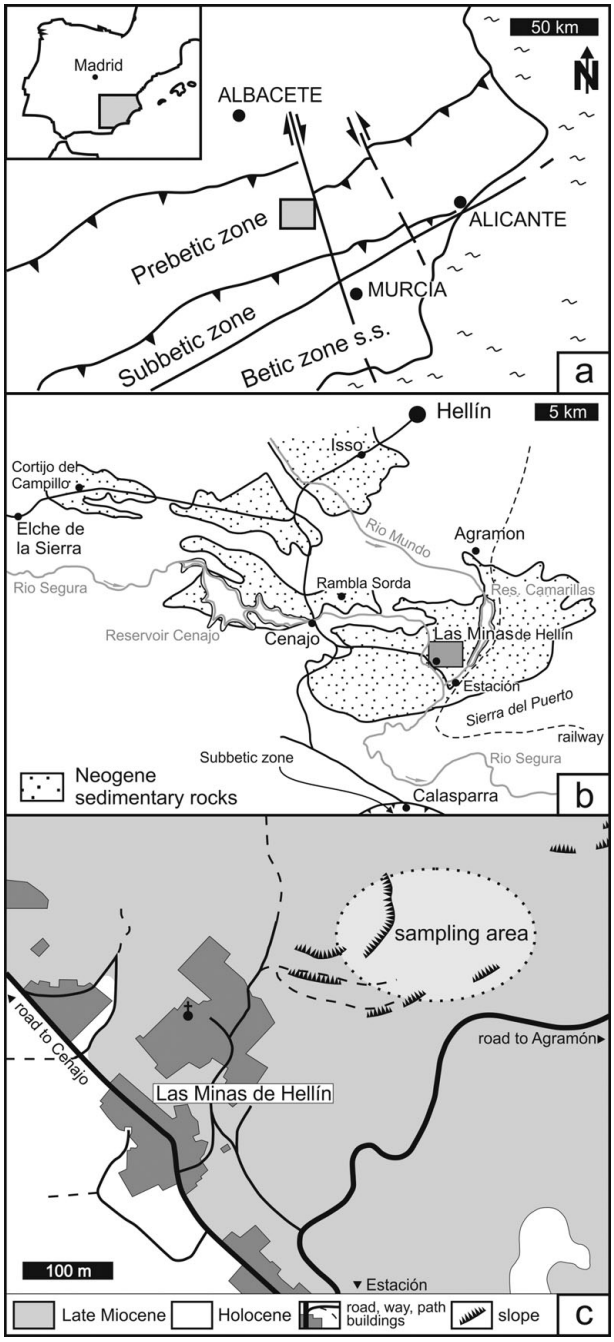

Figure 1. Study area. (a) Location of the Hellín basin in tectonic context of the Betic Chain; modified after Calvo & Elizaga (1989). (b) Sub-basins of the Hellín basin with Neogene sediments; modified after Calvo & Elizaga (1989). (c) Location of the sampling area in the former sulphur mine of Las Minas.

(Navarro Hervás & Rodríguez Estrella, 1985). In the sub-basins of Cenajo and Las Minas, the Las Minas de Hellín Formation contains native sulphur, which was mined until 1960.

For this study, carbonate and gypsum rocks containing native sulphur were collected from the mining area northeast of the small miners' village of Las Minas (Fig. 1c). Sections of evaporites and carbonates are well exposed, but strongly weathered; the samples studied here derived from the upper part of the stratigraphic interval described by Servant-Vildary *et al*.

https://doi.org/10.1017/S0016756811000124 Published online by Cambridge University Press

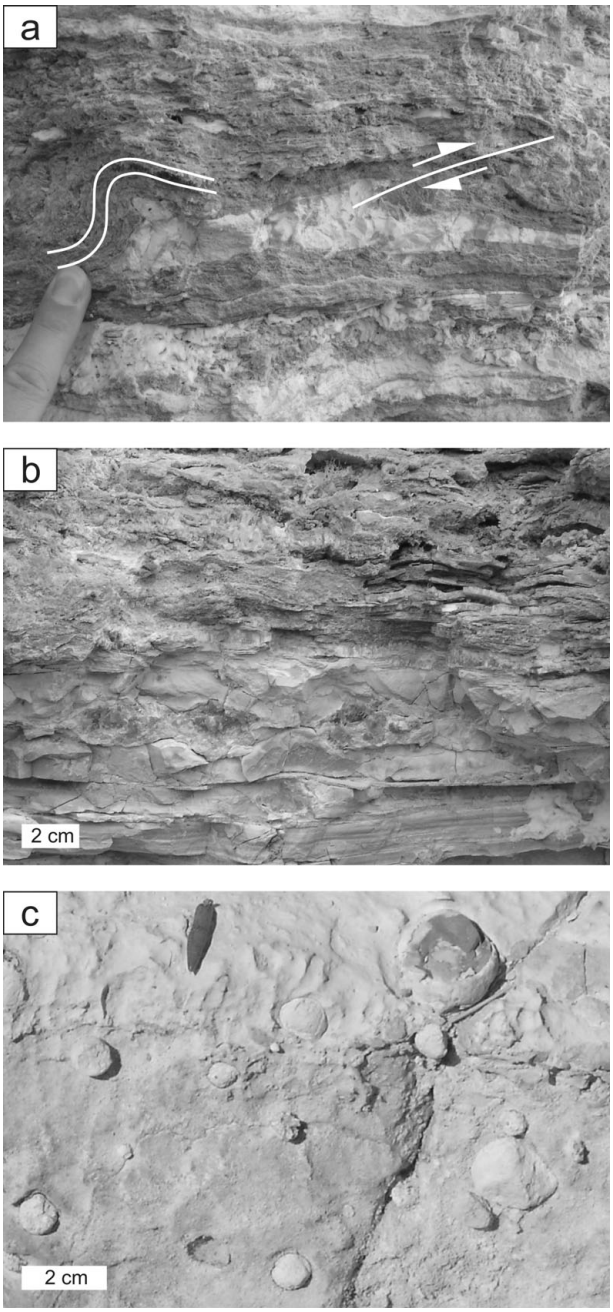

Figure 2. Native sulphur. (a) Sulphur enclosed in secondary gypsum; overlying laminar gypsum beds are bent and faulted (see indication), Las Minas. (b) Sulphur enclosed in carbonate deposits, Las Minas. (c) Sulphur nodules embedded in a carbonate bed, Cenajo. For a colour version of this figure see online Appendix at http://journals.cambridge.org/geo.

(1990). Strata-bound nodules of native sulphur are predominantly embedded in laminated gypsum beds (Fig. 2a) and to a lesser degree in carbonate beds (Fig. 2b). A similar sedimentary sequence is found in the Las Minas de Hellín Formation of the Cenajo sub-basin. The aggregates of native sulphur in the Cenajo sequence resemble those of the Las Minas sequence, although spherical nodules of sulphur have only been recognized in carbonate deposits from Cenajo (Fig. 2c).

3. Methods

Thin-sections were studied with transmitted light and fluorescence microscopy on a Zeiss Axioskop 40 A Pol, equipped with an Axio-Cam MRc digital camera (lamp: HBO 50, filter: BP 365 FT 395 LP 397 and BP 450–490 FT 510 LP 515). Thin-sections were partly stained with combined potassium ferricyanide and alizarin red solution (Füchtbauer, 1988). Scanning-electron microscopy with qualitative element recognition was performed with a Zeiss Supra 40 REM equipped with an Oxford EDX-detector (Inca Penta FETx3).

Mineralogy was determined with a PANalytical X'Pert Pro diffractometer using a Ni-filtered Cu-anode, equipped with a multichannel detector (X'cellerator). Mineral content was estimated semi-quantitatively using the peak areas. Proportions of magnesium to calcium in dolomite were calculated after Lumsden (1979) by quartz-corrected d-values. A LECO CS 200 was used for determination of total organic carbon content.

For stable isotope analyses, mineral phases were drilled from the surface of slabs with a hand-held micro drill. Measurements of carbon and oxygen isotopes (sample weight: 0.02 to 0.10 mg) were performed with a Finnigan MAT 251 mass spectrometer using the Kiel carbonate device type 'Bremen' against natural CO_2 from Burgbohl/Rheinland. A Solenhofen limestone was used as an internal standard, which was calibrated against the international standard NBS 19. Values are reported in the δ-notation relative to the Vienna Pee Dee Belemnite (VPDB) standard. Long-time standard deviation (1σ) for this measurement was ± 0.05 ‰ for $\delta^{13}C$ and ± 0.07 ‰ for $\delta^{18}O$ values. Oxygen isotope values of dolomite were not corrected for different fractionation compared to calcite during precipitation (McKenzie, 1981) or during the analytical procedure (Sharma & Clayton, 1965) because of an undetermined admixture of minor calcite.

For oxygen isotope analysis of sulphate, gypsum was dissolved with sodium chloride solution. After acidification of the solution, sulphate was precipitated as barium sulphate by addition of barium chloride. Sulphur isotopes of gypsum were measured either on gypsum without pre-treatment or on barium sulphate precipitated as above. Samples of sulphur received no pre-treatment for sulphur isotope measurements. Sulphur and oxygen isotope measurements were performed with a Thermo Finnigan mass spectrometer Delta V in a continuous flow setup.

For sulphur isotope analysis, 0.3 mg of barium sulphate, 0.4 mg of calcium sulphate or 0.05 mg of native sulphur (with 1 mg of V_5O_5 as catalyst, respectively) were weighed into tin capsules and combusted in a Euro EA Elemental Analyser (EuroVector, Milan, Italy). The sulphur isotope measurements were calibrated with reference materials NBS 127 and IAEA-SO-6. The sulphur isotopic composition is reported in the δ-notation relative to the Vienna Cañon Diablo Troilite (VCDT) standard. The standard errors (1σ) were less than ± 0.2 ‰ for $\delta^{34}S$ values.

https://doi.org/10.1017/S0016756811000124 Published online by Cambridge University Press

For oxygen isotope analysis, 0.16 mg of barium sulphate was weighed into silver capsules. Under the presence of graphite and glassy carbon, oxygen from sulphate was transferred to carbon monoxide within an elemental analyser (TC/EA, Thermo Fisher Scientific). NBS 127, IAEA-SO-5 and IAEA-SO-6 were used as references for calibration. The oxygen isotopic composition is reported in the δ-notation relative to Vienna Standard Mean Ocean Water (VSMOW). The standard errors (1σ) were less than ± 0.3 ‰ for $\delta^{18}O$ values.

4. Results

4.a. Petrography

4.a.1. Carbonate lithology

Sampled carbonate beds consist predominantly of dolomite with varying amounts of gypsum, calcite and accessory minerals, including clay minerals, feldspars and quartz. Only a few carbonate beds contain more calcite than dolomite. The $MgCO_3$ content of dolomite is generally high (47 to 50 %). The total organic carbon content of carbonate deposits is low to moderate (0.2 to 0.7 %).

Most of the carbonate deposits exhibit a distinct lamination, which can be grouped into three types (Fig. 3). (1) A very regular, varve-like rhythmic lamination is characterized by thin laminae, approximately 0.5 mm in thickness that consist of light-coloured dolomitic microspar and dark organic-rich dolomicrite, respectively (Fig. 3a, b). Where sulphur nodules occur, the lamination is bent and occasionally faulted (Figs 2a, 3a–c). The dolomicrite is partly dissolved or replaced by gypsum, especially in the surroundings of sulphur nodules. Less commonly dolomitic microspar is replaced by gypsum. (2) A second type of lamination is less regular, resembling lamination in microbial mats (Fig. 3d). The carbonate laminae, which differ in thickness, show an uneven surface and wedge out laterally. They are interbedded with discontinuous clay layers. The predominant mineral is dolomite. (3) A third type of lamination comprises dolomite and gypsum laminae of irregular thickness, ranging from a few to 300 μm, accompanied by late diagenetic calcite and chert laminae (Fig. 3e). Plant fragments are common in this lithology.

Beside laminated carbonate beds, dense beds of dolomicrite occur, which are up to a few centimetres in thickness. These beds commonly reveal a clotted (Fig. 4a) or peloidal microfabric. Former cavities, now filled by authigenic minerals, are abundant in this lithology (Fig. 4a). In places the dolomicrite is alternating with dolomitic spar (Fig. 4b). Dolomicritic peloids are up to 30 μm in diameter and are partly recrystallized to microspar along their margins. Peloids tend to form dense fringes around sulphur nodules, which are commonly partly or completely replaced by gypsum (Fig. 4c). Blocky calcite spar with crystals up to 200 μm in diameter is an accessory phase in this lithology.

In different types of dolomitic beds spheroidal dolomite is observed in rock-forming quantities. The pore space left by spheroids is filled by gypsum (Fig. 5a). In some of the vugs, interlayers and surroundings of spheroids, submicroscopic aggregates of clay minerals are present (Fig. 5b). The fluorescent spheroids reveal a dark core of unknown composition surrounded by concentric rings of dolomite (Fig. 5c, d). Spheroids vary between 5 and 10 μm in diameter and are composed of irregularly arranged crystals (Fig. 5e, f).

4.a.2. Native sulphur

Native sulphur occurs as large bright orange to yellow crystals with sharp crystal boundaries (Fig. 6a, b); the crystals are translucent in transmitted light. Sulphur is commonly closely associated with spheroidal dolomite and vugs or fissures filled by secondary gypsum (Fig. 6a, b). Weathered sulphur is bright yellow to whitish in colour (Fig. 2a), shows a powdery consistency, is blurry in transmitted light and is abundantly surrounded by secondary gypsum (Fig. 6c).

In carbonate beds with a varve-like lamination, sulphur aggregates tend to be particularly round (Fig. 3a–c). In carbonate beds of the types 2 and 3 described in the previous Section, lamination is partly interrupted by sulphur nodules. Native sulphur also appears as amoeboidal aggregates (Fig. 6c), possibly filling former cavities, and as tiny accumulations finely dispersed in the host rock (Fig. 6d). Very regular, fluorescent globules with a diameter of approximately 20 μm were recognized in one sample of well-preserved sulphur (Fig. 7).

4.a.3. Gypsum

Gypsum is ubiquitous in the studied sedimentary rocks. In some carbonate beds, gypsum is finely dispersed in the rock matrix. Elsewhere, it represents a secondary mineral, growing as large crystals perpendicular to bedding. Secondary gypsum, which has been described in detail by Servant-Vildary *et al*. (1990), commonly replaces sulphur (Figs 3c, 4c, 6c) and dolomitic microspar. It also fills fissures and vugs in carbonate deposits (Fig. 8). Growth of palisade-like gypsum commonly disturbed the primary lamination. The secondary gypsum of the Las Minas de Hellín sequence closely resembles diagenetic gypsum from the Miocene lacustrine sequence of the Teruel basin in NE Spain (cf. Ortí, Rosell & Anadón, 2010).

4.b. Stable isotopes

4.b.1. Carbon and oxygen isotopes of carbonates

Oxygen isotope values scatter widely from −5.2 to +10.5 ‰ (Table 1; Fig. 9). Dolomite is more enriched in ^{18}O than calcite. Spheroidal dolomite shows slightly

https://doi.org/10.1017/S0016756811000124 Published online by Cambridge University Press

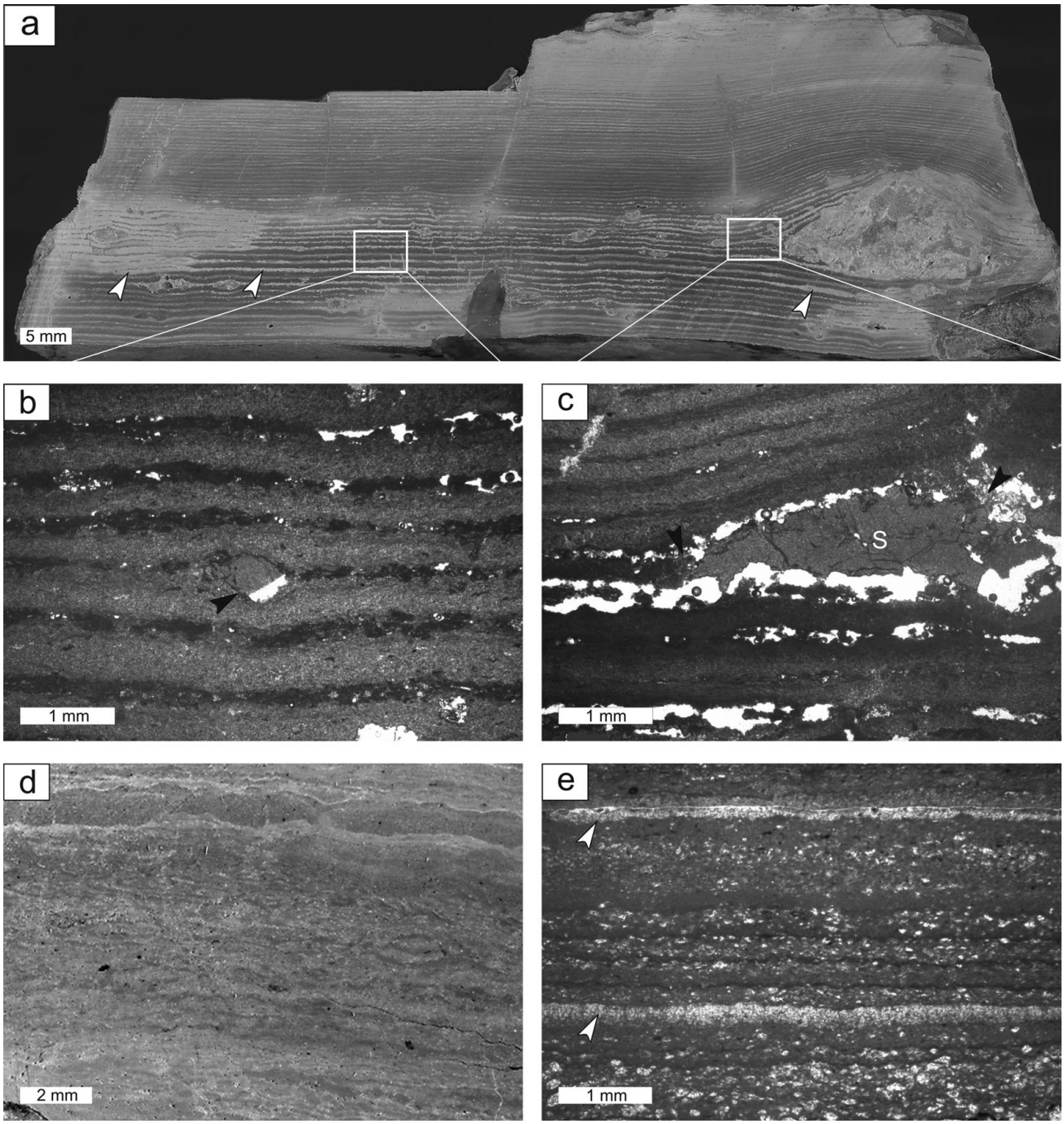

Figure 3. Laminated carbonate beds. (a) Carbonate bed with varved lamination, which is bent around a sulphur nodule; arrowheads indicate laminae of secondary gypsum; scanned slab. (b) Detail of (a), carbonate laminae and small sulphur nodule (arrowhead); plane-polarized light. (c) Detail of (a), bent lamination around a sulphur nodule (S), which is partly dissolved and replaced by diagenetic gypsum (arrowheads); plane-polarized light. (d) Mat-like lamination; plane-polarized light. (e) Irregular lamination with two chert laminae (arrowheads); plane-polarized light.

lower $\delta^{18}O$ values (+6.5 to +9.7 ‰) than other varieties of dolomite (+6.8 to +10.5 ‰). A group of samples with a mixed dolomite and calcite composition exhibits oxygen isotope values close to 0 ‰. The lowest oxygen isotope values are found for late diagenetic calcite (−5.2 to −3.2 ‰).

Most carbon isotope values range from −11.1 to −3.6 ‰. Two samples with slightly higher values (−2.3 ‰) probably reflect reworked marine carbonate. The $\delta^{13}C$ values of samples with a mixed calcite and dolomite composition (−5.3 to −11.1 ‰) as well as the $\delta^{13}C$ values of dolomite (−4.2 to −10.0 ‰) scatter widely. The $\delta^{13}C$ values of dolomite are negatively correlated with the $\delta^{18}O$ values, corresponding to a correlation coefficient of $r = -0.75$ (Fig. 9).

4.b.2. Oxygen isotopes of gypsum and sulphur isotopes of gypsum and native sulphur

Oxygen isotope values of gypsum range from +4.7 to +8.1 ‰ (Table 1; Fig. 10). Native sulphur and

https://doi.org/10.1017/S0016756811000124 Published online by Cambridge University Press

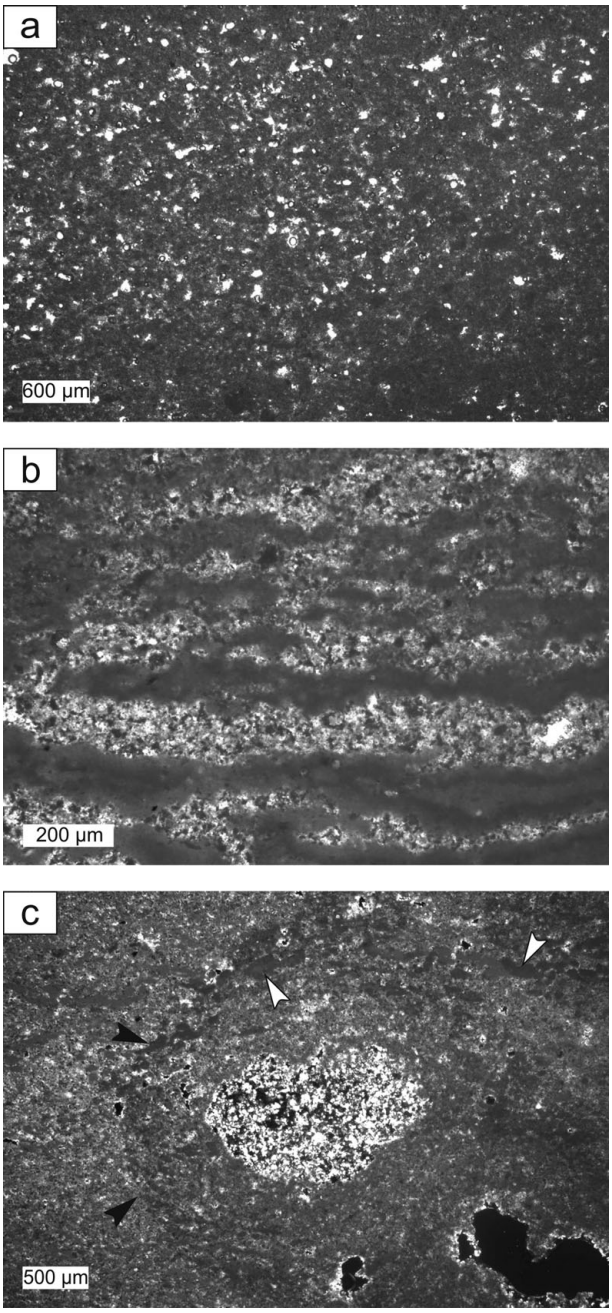

Figure 4. Carbonate deposits. (a) Clotted dolomicrite to microspar; plane-polarized light. (b) Irregular alternation of dolomicrite and microspar; plane-polarized light. (c) Peloidal carbonate with a former sulphur nodule replaced by gypsum surrounded by a dark rim (black arrowheads). White arrowheads point to large peloids; crossed nicols.

secondary gypsum show much lower $\delta^{34}S$ values (−18.2 to −3.7 ‰; Table 1; Figs 10, 11) than primary gypsum of the Las Minas sequence (+13 to +19 ‰; Servant-Vildary *et al*. 1990; Fig. 10). Sulphur isotope values of native sulphur fall into two groups (Fig. 11). One group is less depleted in ^{34}S (−7.8 to −3.7 ‰), whereas the other group shows very low $\delta^{34}S$ values (−17.1 to −13.5 ‰), which are in the same range as values of secondary gypsum (−18.2 to −9.5 ‰). Triassic gypsum sampled from the periphery of the Cenajo sub-basin exhibits a positive sulphur isotope value (+12.0 ‰), in accord with the data of Claypool *et al*. (1980).

5. Discussion

5.a. Formation of authigenic carbonate minerals

In lacustrine environments, carbonate minerals can precipitate from dissolved inorganic carbon (DIC) in the upper water column and accumulate at the lake bottom (Stabel, 1986; Talbot & Kelts, 1990). The carbon isotopic composition of dissolved carbonate in a lacustrine environment is influenced by several factors including the amount and the composition of inflowing water, residence time and lake size (Talbot & Kelts, 1990; Lee, McKenzie & Sturm, 1987). Furthermore, the $\delta^{13}C$ values of DIC can shift towards higher values owing to primary production inside the lake and evaporation (Talbot, 1990). In closed lakes, $\delta^{13}C$ values of primary carbonates usually range from –5 to +3 ‰ (McKenzie, 1985; Talbot, 1990; Talbot & Kelts, 1990; Tenzer, Meyers & Knoop, 1997). The Miocene Hellín lake was most likely hypersaline, because Late Miocene climatic conditions favoured evaporation in the Mediterranean area (van Dam & Weltje, 1999; García-Alix *et al*. 2008) and abundant Miocene evaporites are present in the Hellín basin. The variable $\delta^{18}O$ values of the studied carbonates reflect the strong influence of inflow and evaporation, which is typical for hydrologically closed lakes (cf. Talbot & Kelts, 1990).

Apart from formation in the water column, early diagenesis in lacustrine sediments can induce carbonate precipitation as well. As a consequence of anaerobic remineralization of organic matter, in particular bacterial sulphate reduction, carbonate alkalinity commonly increases (Abd-El-Malek & Rizk, 1963*a*,*b*; van Lith *et al*. 2003). The resulting authigenic carbonate minerals are characterized by low $\delta^{13}C$ values depending on the source of fresh organic matter or fossil hydrocarbons (Irwin, Curtis & Coleman, 1977; Peckmann & Thiel, 2004). The $\delta^{13}C$ values of higher land plants (as low as −34 ‰) tend to be lower than that of freshwater algae (−23 ‰; Smith & Epstein, 1971). Because of the preferential uptake of ^{12}C-enriched compounds during microbial remineralization, the produced carbonate is even more depleted in ^{13}C than the source material (e.g. Lee, McKenzie & Sturm, 1987). The carbon isotopic composition of the Hellín basin carbonate deposits (as low as −11 ‰; Fig. 9), thus, reflects a combination of lake water DIC and carbonate alkalinity produced by the remineralization of organic matter. Dolomite from the Cenajo sub-basin of the Hellín basin and the Lorca basin reveal similar $\delta^{13}C$ values, which have been attributed to bacterial sulphate reduction (Bellanca *et al*. 1989; Rouchy *et al*. 1998).

Additional evidence for a microbial origin of the Hellín basin dolomites stems from the anticorrelation between $\delta^{13}C$ and $\delta^{18}O$ values (Fig. 9). During phases of enhanced evaporation the sulphate concentration

https://doi.org/10.1017/S0016756811000124 Published online by Cambridge University Press

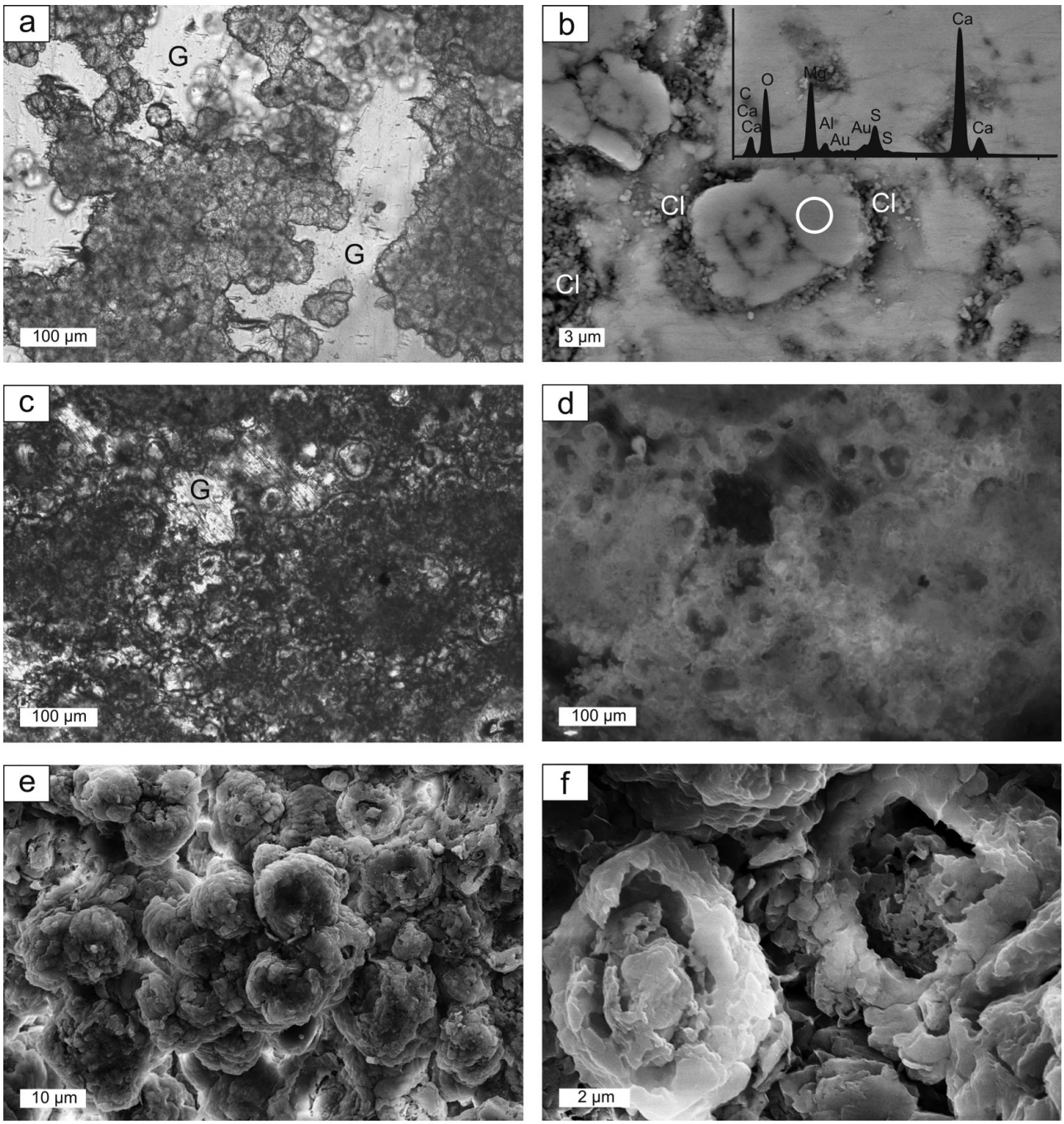

Figure 5. Spheroidal dolomite. G – gypsum. (a) Spheroidal dolomite with gypsum; plane-polarized light. (b) Spheroidal dolomite and associated clay minerals (Cl); SEM micrograph of thin-section; circle displays area of EDX-measurement, spectrum with counts from 0 to 5 keV, gold peak from coating. (c) Spheroidal dolomite with gypsum; plane-polarized light. (d) Same detail as (c); note autofluorescence of spheroids; fluorescence image. (e) Aggregate of spheroidal dolomite; SEM micrograph. (f) Close-up view of two spheroids; SEM micrograph.

in the lake water increased, allowing sulphate ions to penetrate deeper into the sediment, which consequently expanded the sulphate reduction zone (cf. Kasten & Jørgensen, 2000). When this happened, sulphate reduction overprinted carbonate beds by inducing the interstitial precipitation of ^{18}O-enriched and ^{13}C-depleted dolomite, with ^{18}O enrichment reflecting a high degree of evaporation and ^{13}C depletion corresponding to a high contribution of carbonate derived from bacterial sulphate reduction coupled to oxidation of organic matter, crude oil or methane.

An anoxic milieu in the lacustrine sediments of the Hellín basin, which is required for sulphate reduction, agrees with the lack of bioturbation as revealed by the undisturbed lamination in the sulphur-bearing strata. The absence of replacive growth supports an early origin of dolomite (cf. Servant-Vildary *et al*. 1990). The biological origin of the studied dolomite – resulting from microbially induced precipitation and not from dolomitization – is evidenced by microfabrics such as mat-like lamination, aggregates of clotted or peloidal dolomicrite and particularly spheroidal dolomite. The

https://doi.org/10.1017/S0016756811000124 Published online by Cambridge University Press

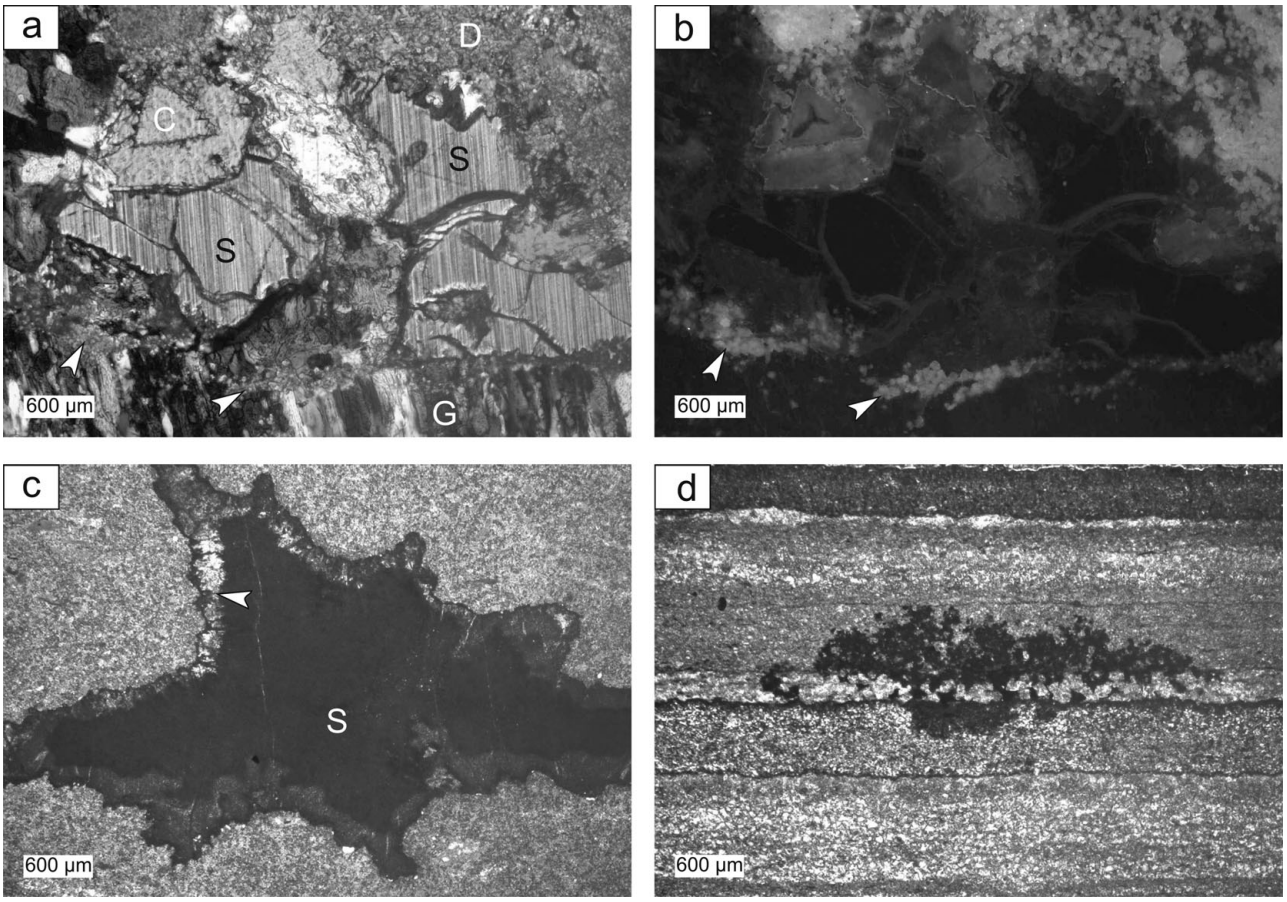

Figure 6. Native sulphur. C – carbonate; D – dolomite; G – gypsum; S – native sulphur. (a) Well-preserved sulphur surrounded by spheroidal dolomite (arrowheads); gypsum-filled fissure in the lower part of the photomicrograph; plane-polarized light. (b) Same detail as (a), note fluorescence of spheroidal dolomite (arrowheads); fluorescence image. (c) Slightly weathered aggregate of sulphur with a rim of gypsum (arrowhead); plane-polarized light. (d) Minor accumulation of sulphur in a laminated carbonate bed; plane-polarized light.

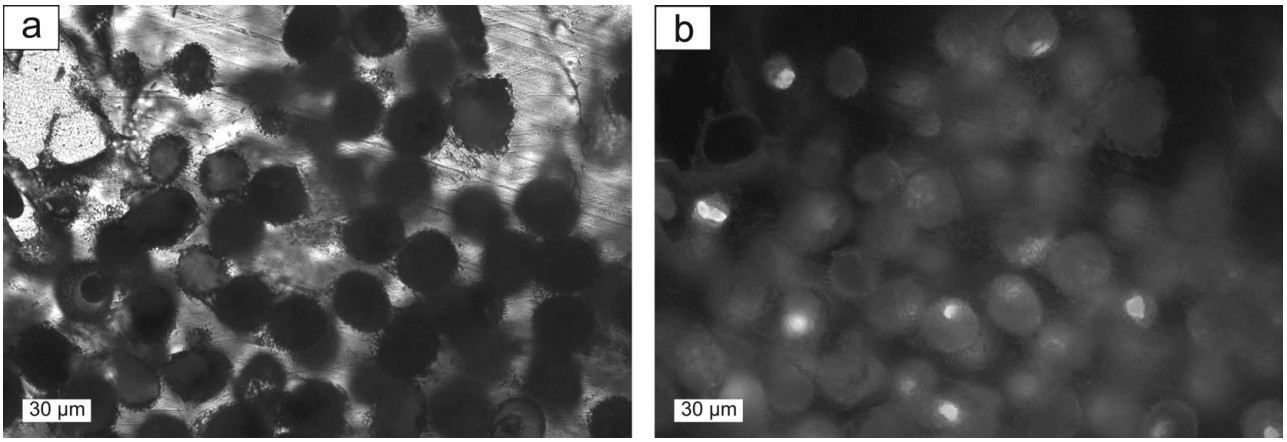

Figure 7. (a) Putative fossilized bacteria enclosed in sulphur; plane-polarized light. (b) Same detail as (a); fluorescence image.

strong fluorescence of the spheroids indicates a high content of organic matter (cf. Dravis & Yurewicz, 1985). Notably, spheroidal dolomite has been suggested to result from the bacterial remineralization of organic matter (Lalou, 1957; Gunatilaka, 1989; Ayllón-Quevedo *et al*. 2007; Sanz-Montero, Rodríguez-Aranda & García del Cura, 2009), indicating that this fabric is typical for microbial dolomite. Similar fabrics have been observed in microbial dolomite forming in modern lagoonal environments (Vasconcelos & McKenzie, 1997; Wright, 1999). The shape of spheroids is believed to reflect microenvironments of mineral precipitation, where cells and extracellular polymeric substances act as nucleation sites (Vasconcelos *et al*. 1995; Burns, McKenzie & Vasconcelos, 2000; van Lith *et al*. 2003; Ayllón-Quevedo *et al*. 2007; Dupraz *et al*. 2008).

High sulphate concentrations were found to inhibit dolomite precipitation (e.g. Baker & Kastner, 1981;

https://doi.org/10.1017/S0016756811000124 Published online by Cambridge University Press

Table 1. Stable isotopes in carbonate deposits, native sulphur and secondary gypsum of Las Minas de Hellín and one sample of Triassic gypsum from near Cenajo

	Carbonate			Sulphate & sulphur		
Sample	$\delta^{13}C$ [‰ VPDB]	$\delta^{18}O$ [‰ VPDB]	texture/mineralogy	$\delta^{34}S$ [‰ VCDT]	$\delta^{18}O$ [‰ VSMOW]	texture/mineralogy
H 1	−7.9	10.2	peloidal dolomite	−14.4	4.7	gypsum filled fissure
H 1	−7.9	9.9	peloidal dolomite			
H 1	−7.8	10.5	peloidal dolomite			
H 1	−7.1	10.0	peloidal dolomite			
H 1	−7.1	9.7	spheroidal dolomite			
H 3				−13.0	8.1	gypsum, substituted sulphur nodule
H 3				−17.1		gypsum, substituted sulphur nodule
H 5A	−7.0	10.3	laminated dolomite	−3.7		native sulphur
H 5A	−7.1	10.1	laminated dolomite	−7.0		native sulphur
H 5A	−7.2	9.8	laminated dolomite			
H 5B	−7.1	10.1	laminated dolomite	−4.3		native sulphur
H 5B	−7.2	10.1	laminated dolomite	−3.7		native sulphur
H 5B	−7.1	10.1	laminated dolomite			
H 6A	−5.0	6.8	microsparitic dolomite	−11.1	6.0	gypsum filled fissure
H 6A	−5.7	7.1	microsparitic dolomite	−12.8	6.3	gypsum filled fissure
H 6A	−6.0	7.9	spheroidal dolomite			
H 6A	−5.8	7.4	spheroidal dolomite			
H 6B	−5.3	6.5	spheroidal dolomite	−18.2		gypsum, rim around native sulphur
H 6B	−5.0	6.5	spheroidal dolomite	−6.7		native sulphur
H 6B				−6.3		native sulphur
H 7	−8.6	9.5	micritic dolomite			
H 7	−8.9	9.6	micritic dolomite			
H 8	−8.5	9.9	microsparitic dolomite			
H 8	−8.5	9.5	microsparitic dolomite			
H 8	−7.3	9.3	clotted dolomite			
H 8	−7.5	9.1	clotted dolomite			
H 8	−7.6	8.9	microsparitic/clotted dolomite			
H 8	−7.7	9.1	microsparitic/clotted dolomite			
H 9A	−6.6	−0.3	matrix calcite & dolomite	−13.5		native sulphur
H 9A	−6.2	−0.3	matrix calcite & dolomite	−12.3		gypsum, rim around native sulphur
H 9A	−6.4	0.6	peloidal dolomite & calcite			
H 9A	−5.3	0.7	clotted dolomite & calcite			
H 9A	−5.5	1.2	clotted dolomite & calcite			
H 9B				−7.8		native sulphur
H 9B				−15.0		native sulphur
H 12	−6.5	8.3	peloidal dolomite	−15.3		gypsum, inside chert layer
H 12	−4.2	6.2	microsparitic dolomite	−14.3	7.6	gypsum filled fissure
H 12				−15.0	7.6	gypsum filled fissure
H 13A	−5.6	7.2	clotted dolomite	−9.5		gypsum filled cavity
H 13A	−4.7	6.5	clotted dolomite			
H 13B				−7.0		native sulphur
H 14	−11.1	2.2	matrix calcite			
H 14	−9.6	1.1	matrix calcite			
H 14	−3.6	−3.9	microsparitic calcite			
H 15	−2.3	0.2	matrix calcite (marine reworked)			
H 15	−2.3	0.5	matrix calcite (marine reworked)			
H 16	−8.1	−0.2	matrix calcite & dolomite	−11.3	5.2	gypsum, inside lamination
H 16	−8.6	1.5	matrix calcite & dolomite	−12.6	6.1	gypsum, inside lamination
H 19	−6.8	−3.2	microsparitic calcite	−15.7		native sulphur
H 19	−6.9	−3.4	microsparitic calcite			
H 19	−6.5	−3.7	microsparitic calcite			
H 20.1	−9.8	10.0	microsparitic dolomite			
H 20.1	−9.9	9.7	microsparitic dolomite	−7.8		native sulphur
H 20.1	−10.0	9.9	microsparitic dolomite			
H 20.1	−9.6	9.1	microsparitic dolomite	−11.4	5.0	gypsum filled fissure
H 20.1	−6.8	−3.4	sparitic calcite	−11.9	5.2	gypsum filled fissure
H 20.1	−6.6	−5.2	sparitic calcite	−13.4		gypsum filled fissure
H 20.1	−9.7	8.8	microsparitic dolomite			
H 21				−17.1		native sulphur
H 21				−14.2		native sulphur
H 21				−11.9	7.5	gypsum, substituted lamination
H 21				−11.6	7.9	gypsum, substituted lamination
Triassic gypsum (near Cenajo)				12.0	11.7	gypsum

for an opposing view see Sánchez-Román *et al*. 2009). Dolomite forms under surface conditions when bacterial sulphate reduction effectively reduces sulphate concentration (Baker & Kastner, 1981; Vasconcelos & McKenzie, 1997; Wright & Wacey, 2005). Sulphate-reducing bacteria are believed to favour dolomite formation by the liberation of magnesium ions, which are efficiently complexed by sulphate ions (Slaughter & Hill, 1991; Vasconcelos *et al*. 1995; Vasconcelos & McKenzie, 1997). A magnesium to calcium ratio of

https://doi.org/10.1017/S0016756811000124 Published online by Cambridge University Press

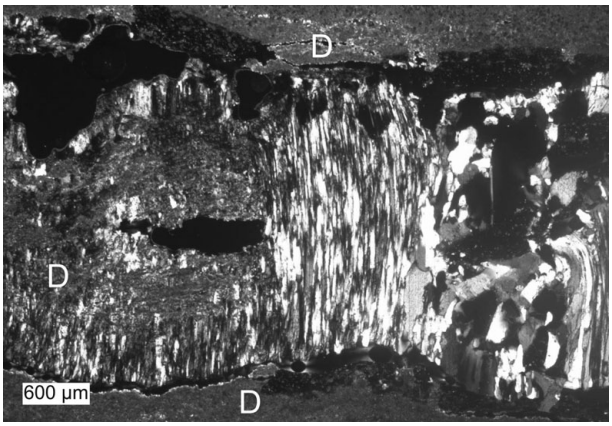

Figure 8. Fissure filled with fibrous gypsum (centre), blocky gypsum (right) and minor dolomite (D) derived from the rock matrix.

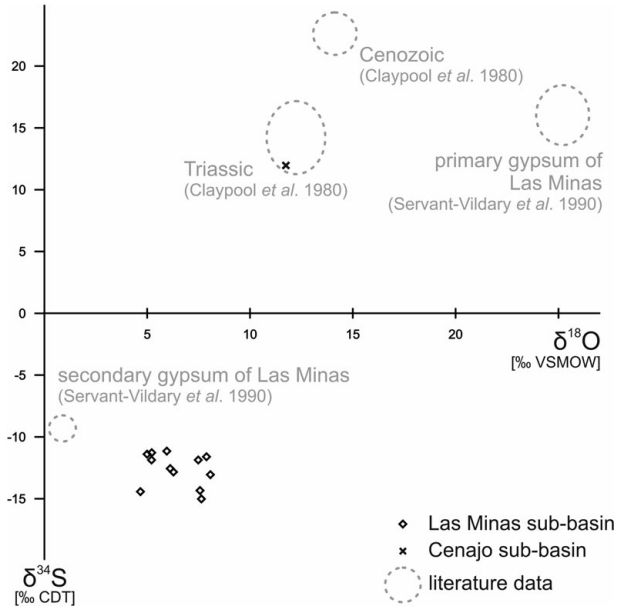

Figure 10. Stable sulphur and oxygen isotope values of secondary gypsum from Las Minas de Hellín and Triassic gypsum from Cenajo. Triassic and Cenozoic marine sulphate for comparison.

5:1 to 10:1 has been found to be necessary for dolomite precipitation (e.g. Folk & Land, 1975; Warren, 2000). In lacustrine environments such high Mg:Ca ratios can be achieved (1) by consumption of calcium ions during gypsum precipitation (Folk & Land, 1975; Hardie, 1987), (2) by precipitation of calcite (Land, 1998) or (3) during early diagenesis of clay minerals with a release of magnesium ions (Kahle, 1965; Weaver & Beck, 1971). Whereas the latter process has been suggested to have played a significant role during the precipitation of dolomite spheroids in Kuwait (Khalaf, 1990), the first factor and, to a lesser degree, the second factor probably favoured dolomite formation in the Hellín basin.

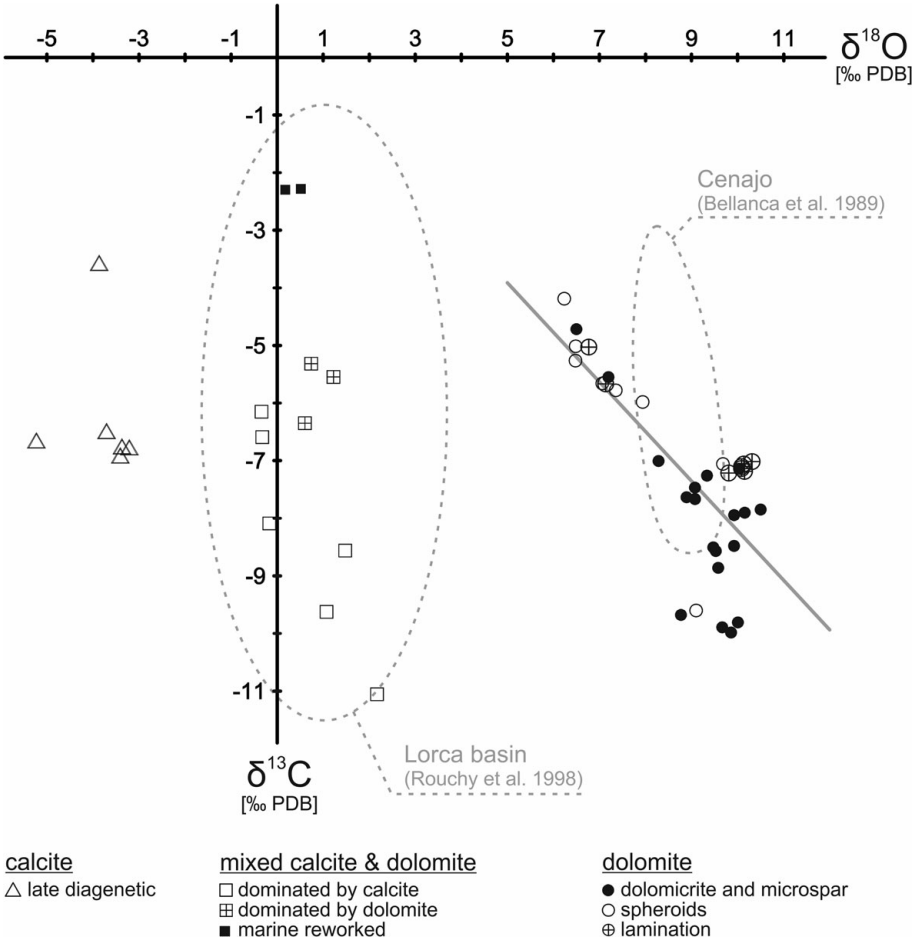

Figure 9. Stable carbon and oxygen isotope values of carbonate deposits of Las Minas de Hellín. Trend line indicates linear regression of dolomite values. Fields defined by dotted lines indicate composition of carbonates from the Lorca and Cenajo basins.

https://doi.org/10.1017/S0016756811000124 Published online by Cambridge University Press

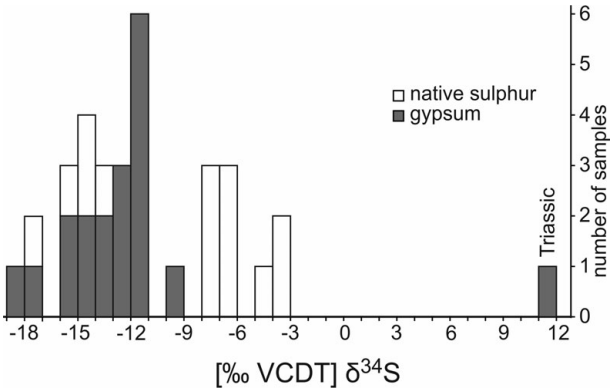

Figure 11. Stable sulphur ($\delta^{34}S$) isotope values of Neogene secondary gypsum and native sulphur from Las Minas de Hellín and Triassic gypsum from Cenajo.

Variations in lake water chemistry are a possible cause for the changes from calcite to dolomite lithologies in the sedimentary strata of the Hellín basin (cf. Servant-Vildary *et al*. 1990). Such a scenario has been described for the Devonian Orcadian basin and the modern Lagoa Vermelha, where dolomite formation is believed to be linked to periods of enhanced evaporation, and calcite formation supposedly takes place during periods of enhanced freshwater input (Janaway & Parnell, 1989; Vasconcelos & McKenzie, 1997). High $\delta^{18}O$ values of Hellín basin dolomites (+6.2 to +10.5 ‰) confirm that dolomite precipitated in an environment typified by evaporation (cf. Talbot & Kelts, 1990), as the highest calculated value for calcite would still be +7.1 ‰ after the correction for different fractionation factors during precipitation ($\varepsilon^{18}O_{dolomite-calcite} = +2.6$ ‰; Vasconcelos *et al*. 2005) and for fractionation during the analytical procedure ($\varepsilon^{18}O_{dolomite-calcite} = +0.8$ ‰ at 25 °C; Sharma & Clayton, 1965). Carbonate deposits with a mixed composition of calcite and dolomite and $\delta^{18}O$ values close to 0 ‰ probably reflect periods of dilution of the lake by freshwater, whereas calcite spar with negative $\delta^{18}O$ values precipitated from meteoric waters during late diagenesis.

5.b. Formation of native sulphur and secondary gypsum

Microbial sulphate reduction releases hydrogen sulphide, which is further oxidized to native sulphur in some settings (e.g. Machel, 1992). Sulphate-reducing bacteria discriminate against ^{34}S, resulting in the formation of hydrogen sulphide with low $\delta^{34}S$ values (e.g. Kaplan & Rittenberg, 1964; Canfield, 2001). Similar to other basins in Spain like the Teruel basin, the Ebro basin or basins in the eastern Betics (Anadón, Rosell & Talbot, 1992; Utrilla *et al*. 1992; Playà, Ortí & Rosell, 2000), Triassic evaporitic rocks with an average $\delta^{34}S$ value of +12 ‰ are present in the drainage area of the Hellín basin (Servant-Vildary *et al*. 1990). During Miocene time, the Triassic evaporites were dissolved by meteoric waters and the resultant sulphate ions were subjected to bacterial sulphate reduction in the Hellín basin. The primary gypsum of the lacustrine sedimentary sequence of the Hellín basin is slightly enriched in ^{34}S compared to Triassic gypsum (+13 to +19 ‰; Servant-Vildary *et al*. 1990), reflecting the removal of isotopically light sulphate by bacterial sulphate reduction. The oxidation of sulphide to sulphur involves only a negligible fractionation effect for sulphur isotopes (Canfield, 2001; Hoefs, 2004). Therefore, the low $\delta^{34}S$ values of native sulphur from the Hellín basin (−17.1 to −3.7 ‰) reflect the isotopic composition of sulphide produced by bacterial sulphate reduction. The accordant fractionation of sulphur isotopes between sulphate and sulphide (14 to 30 ‰) is well within the known range of bacterial sulphate reduction (Hartmann & Nielsen, 1969; Goldhaber & Kaplan, 1974; Bolliger *et al*. 2001; Detmers *et al*. 2001).

The oxidation of hydrogen sulphide to native sulphur occurs abiologically or biologically (Machel, 1992). One observation suggests that at least part of the native sulphur of the Hellín basin results from biological oxidation. The fluorescent globules enclosed in native sulphur (Fig. 7) probably represent fossilized bacterial cells. They resemble the sulphide-oxidizing bacteria *Thiomargarita* sp. or *Achromatium* sp. (pers. comm. H. N. Schulz-Vogt, 2009). *Thiomargarita* sp. have been exclusively described from marine sediments (Schulz & Schulz, 2005). Their metabolism is based on oxidation of sulphide with oxygen or nitrate (Schulz & Jørgensen, 2001; Schulz, 2002). *Achromatium* spp., however, prefer lacustrine conditions and gain energy by the oxidation of sulphide to sulphate with native sulphur as an intermediate (Gray *et al*. 1999). The bending of sediment layers around sulphur nodules points to a syngenetic formation of sulphur and, thus, agrees with biological oxidation of hydrogen sulphide.

Most of the gypsum in the Las Minas de Hellín Formation is obviously of a diagenetic origin, resembling diagenetic gypsum of the Miocene Teruel basin (cf. Ortí, Rosell & Anadón, 2010). Such an origin is revealed by the replacement of sulphur nodules or carbonate laminae and the infilling of late fissures. The oxidation of reduced sulphur species produces sulphuric acid, which causes a drop in pH leading to carbonate dissolution (Boudreau, 1991; Walter *et al*. 1993; Ku *et al*. 1999; Pirlet *et al*. 2010). The gypsum that tends to precipitate under these conditions replaces carbonate and native sulphur in the sedimentary sequence (Servant-Vildary *et al*. 1990). The fractionation effect for sulphur isotopes during the precipitation of gypsum (1.6 ‰) is small (Nakai & Jensen, 1964; Thode & Monster, 1973; Claypool *et al*. 1980). The low $\delta^{34}S$ values (–18.2 to –9.5 ‰) of diagenetic gypsum consequently confirm its origin from the oxidation of native sulphur. This secondary gypsum is also characterized by low $\delta^{18}O$ values, reflecting the uptake of oxygen derived from meteoric waters (cf. Taylor & Wheeler, 1984; Brunner *et al*. 2005).

https://doi.org/10.1017/S0016756811000124 Published online by Cambridge University Press

6. Conclusions

The native sulphur and authigenic dolomite present in the lacustrine evaporitic sequence of the Late Miocene Las Minas de Hellín Formation of the Hellín basin in SE Spain formed as a consequence of bacterial sulphate reduction. The high sulphate concentration of the Miocene lake led to the deposition of primary lacustrine gypsum and served as an electron acceptor for bacterial remineralization of organic matter. A microbial origin of authigenic dolomite is confirmed by its $\delta^{13}C$ values as low as −10 ‰ and textural evidence including spheroids, clotted and peloidal fabrics, as well as mat-like lamination. Microfossils preserved in native sulphur indicate that hydrogen sulphide produced by the sulphate-reducing bacteria was at least partially oxidized biologically, resulting in sulphur formation. The putative bacterial fossils resemble the sulphide-oxidizing bacteria *Thiomargarita* and *Achromatium*. A significant amount of the native sulphur in the Las Minas de Hellín Formation was later oxidized to ^{34}S-depleted secondary gypsum ($\delta^{34}S$ values as low as −18 ‰), still reflecting the sulphur isotope composition of the biogenic sulphur ($\delta^{34}S$ values as low as −17 ‰).

Acknowledgements. We thank Sebastian Flotow (Bremen) for thin-section preparation, Brit Kockisch (Bremen) for TOC measurements, Thomas Max (MPI Bremen) for help with sulphur and oxygen isotope analysis, Monika Segl (Bremen) for carbon and oxygen isotope analysis, Christoph Vogt (Bremen) for XRD measurements, Petra Witte (Bremen) for help with REM analysis and Heide Schulz-Vogt (MPI Bremen) for comments on sulphide-oxidizing bacteria. Comments by Federico Ortí (Barcelona) and an anonymous referee helped improve the manuscript. This project was supported by the DFG Research Centre 'The ocean in the Earth system', the international graduate college EUROPROX and the Max Planck Society.

References

ABD-EL-MALEK, Y. & RIZK, S. G. 1963*a*. Bacterial sulphate reduction and development of alkalinity. I. Experiments with synthetic media. *Journal of Applied Bacteriology* **26**, 7–13.

ABD-EL-MALEK, Y. & RIZK, S. G. 1963*b*. Bacterial sulphate reduction and development of alkalinity. II. Laboratory experiments with soils. *Journal of Applied Bacteriology* **26**, 14–19.

ANADÓN, P., ROSELL, L. & TALBOT, M. R. 1992. Carbonate replacement of lacustrine gypsum deposits in two Neogene continental basins, eastern Spain. *Sedimentary Geology* **78**, 201–16.

AYLLÓN-QUEVEDO, F., SOUZA-EGIPSY, V., SANZ-MONTERO, M. E. & RODRÍGUEZ-ARANDA, J. P. 2007. Fluid inclusion analysis of twinned selenite gypsum beds from the Miocene of the Madrid basin (Spain). Implication on dolomite bioformation. *Sedimentary Geology* **201**, 212–30.

BAKER, P. A. & KASTNER, M. 1981. Constraints on the formation of sedimentary dolomite. *Science* **213**, 214–16.

BELLANCA, A., CALVO, J. P., CENSI, P., ELIZAGA, E. & NERI, R. 1989. Evolution of lacustrine diatomite carbonate cycles of Miocene age, southeastern Spain: petrology and isotope geochemistry. *Journal of Sedimentary Petrology* **59**, 45–52.

BOLLIGER, C., SCHROTH, M. H., BERNASCONI, S. M., KLEIKEMPER, J. & ZEYER, J. 2001. Sulfur isotope fractionation during microbial sulfate reduction by toluene-degrading bacteria. *Geochimica et Cosmochimica Acta* **65**, 3289–98.

BÖTTCHER, M. E. & PARAFINIUK, J. 1998. Methane-derived carbonates in a native sulfur deposit: stable isotope and trace element discriminations related to the transformation of aragonite to calcite. *Isotopes in Environmental and Health Studies* **34**, 177–90.

BOUDREAU, B. P. 1991. Modelling the sulfide-oxygen reaction and associated pH gradients in porewaters. *Geochimica et Cosmochimica Acta* **55**, 145–59.

BRUNNER, B., BERNASCONI, S. M., KLEIKEMPER, J. A. & SCHROTH, M. H. 2005. A model for oxygen and sulfur isotope fractionation in sulfate during bacterial sulfate reduction processes. *Geochimica et Cosmochimica Acta* **69**, 4773–85.

BURNS, S. J., MCKENZIE, J. A. & VASCONCELOS, C. 2000. Dolomite formation and biogeochemical cycles in the Phanerozoic. *Sedimentology* **47**, 49–61.

CALVO, J. P. & ELIZAGA, E. 1989. Sedimentación evaporítica en las cuencas de Cenajo y Las Minas – Camarillas (región de Hellín, Mioceno Superior del área Prebética). In *Formaciones evaporíticas de la Cuenca del Ebro y cadenas periféricas, y de la zona de Levante* (eds F. Ortí & J. M. Salvany), pp. 246–50. Barcelona: University of Barcelona.

CALVO, J. P., ELIZAGA, E., LOPEZ MARTINEZ, N., ROBLES, F. & USERA, J. 1978. El Mioceno superior continental del Prébetico Externo: Evolución del Estrecho Nordbético. *Boletín Geológico y Minero* **89**, 407–26.

CANFIELD, D. E. 2001. Biogeochemistry of sulfur isotopes. In *Stable Isotope Geochemistry. Mineralogical Society of America & Geochemical Society: Reviews in Mineralogy and Geochemistry* (eds J. W. Valley & D. R. Cole), pp. 607–36. Washington, DC: Mineralogical Society of America.

CASTANIER, S., LE MÉTAYER-LEVREL, G., PERTHUISOT, J. P. 1999. Ca-carbonate precipitation and limestone genesis – the microbiogeologist point of view. *Sedimentary Geology* **126**, 9–23.

CERLING, T. E., BOWMAN, J. R. & O'NEIL, J. R. 1988. An isotopic study of a fluvial-lacustrine sequence: the Plio-Pleistocene Koobi Fora sequence, East Africa. *Palaeogeography, Palaeoclimatology, Palaeoecology* **63**, 335–56.

CLAYPOOL, G. E., HOLSER, W. T., KAPLAN, I. R., SAKAI, H. & ZAK, I. 1980. The age curves of sulfur and oxygen isotopes in marine sulfate and their mutual interpretation. *Chemical Geology* **28**, 199–260.

DAVIS, J. B. & KIRKLAND, D. W. 1979. Bioepigenetic sulfur deposits. *Economic Geology and the Bulletin of the Society of Economic Geologists* **74**, 462–8.

DESSAU, G., JENSEN, M. L. & NAKAI, N. 1962. Geology and isotopic studies of Sicilian sulfur deposits. *Economic Geology* **57**, 410–38.

DETMERS, J., BRÜCHERT, V., HABICHT, K. S. & KUEVER, J. 2001. Diversity of sulfur isotope fractionations by sulfate-reducing prokaryotes. *Applied and Environmental Microbiology* **67**, 888–94.

DRAVIS, J. J. & YUREWICZ, D. A. 1985. Enhanced carbonate petrography using fluorescence microscopy. *Journal of Sedimentary Petrology* **55**, 795–804.

DUPRAZ, C., REID, R. P., BRAISSANT, O., DECHO, A. W., NORMAN, R. S. & VISSCHER, P. T. 2008. Processes of carbonate precipitation in modern microbial mats. *Earth Science Reviews* **96**, 141–62.

FEELY, H. W. & KULP, J. L., 1957. Origin of Gulf coast salt-dome sulphur deposits. *Bulletin of the American Association of Petroleum Geologists* **41**, 1802–53.

FOLK, R. L. & LAND, L. S. 1975. Mg/Ca ratio and salinity: two controls over crystallization of dolomite. *Bulletin of the American Association of Petroleum Geologists* **59**, 60–8.

FÜCHTBAUER, H. 1988. *Sedimente und Sedimentgesteine*, 4th ed. Stuttgart: Schweizerbart'sche Verlagsbuchhandlung, 1141 pp.

GARCÍA-ALIX, A., MINWER-BARAKAT, R., SUÁREZ, E. M., FREUDENTHAL, M. & MARTÍN, J. M. 2008. Late Miocene–Early Pliocene climatic evolution of the Granada Basin (southern Spain) deduced from the paleoecology of the micromammal associations. *Palaeogeography, Palaeoclimatology, Palaeoecology* **265**, 214–25.

GARCIA DOMINGO, A., LOPEZ OLMEDO, F., JEREZ MIR, L. & GALLEGO COIDURAS, I. 1980. Mapa Geológico de España, hoja 868 Isso, Escala 1:50.000. Instituto Geológico y Minero de España.

GIESE, P., REUTTER, K. J., JACOBSHAGEN, V. & NICOLICH, R. 1982. Explosion seismic crustal studies in the Alpine Mediterranean region and their implications to tectonic processes. In *Alpine Mediterranean Geodynamics* (eds H. Berckhemer & K. J. Hsü), pp. 39–73. Washington, DC: American Geophysical Union.

GOLDHABER, M. B. & KAPLAN, I. R. 1974. The sedimentary sulphur cycle. In *The Sea* (ed. E. B. Goldberg), pp. 569–655. New York: Wiley.

GRAY, N. D., HOWARTH, R., PICKUP, R. W., GWYN JONES, J. & HEAD, I. M. 1999. Substrate uptake by uncultured bacteria from the genus *Achromatium* determined by microautoradiography. *Applied and Environmental Microbiology* **65**, 5100–6.

GUNATILAKA, A. 1989. Spheroidal dolomites – origin by hydrocarbon seepage? *Sedimentology* **36**, 701–10.

HARDIE, L. A. 1987. Dolomitization; a critical view of some current views. *Journal of Sedimentary Petrology* **57**, 166–83.

HARTMANN, M. & NIELSEN, H. 1969. δ^{34}S-Werte in rezenten Meeressedimenten und ihre Deutung am Beispiel einiger Sedimentprofile aus der westlichen Ostsee. *Geologische Rundschau* **58**, 621–55.

HENTZ, T. F. & HENRY, C. D. 1989. Evaporite-hosted native sulfur in Trans-Pecos Texas: relation to late-phase Basin and Range deformation. *Geology* **17**, 400–3.

HOEFS, J. 2004. *Stable Isotope Geochemistry*, 5th ed. Berlin: Springer, 244 pp.

IRWIN, H., CURTIS, C. & COLEMAN, M. 1977. Isotopic evidence for source of diagenetic carbonates formed during burial of organic-rich sediments. *Nature* **269**, 209–13.

JANAWAY, T. M. & PARNELL, J. 1989. Carbonate production within the Orcadian basin, northern Scotland: a petrographic and geochemical study. *Palaeogeography, Palaeoclimatology, Palaeoecology* **70**, 89–105.

JASSIM, S. Z., RAISWELL, R. & BOTTRELL, S. H. 1999. Genesis of the Middle Miocene stratabound sulphur deposits of northern Iraq. *Journal of the Geological Society, London* **156**, 25–39.

JOLIVET, L., AUGIER, R., ROBIN, C., SUC, J.-P. & ROUCHY, J. M. 2006. Lithospheric-scale geodynamic context of the Messinian salinity crisis. *Sedimentary Geology* **188–189**, 9–33.

KAHLE, C. F. 1965. Possible roles of clay minerals in the formation of dolomite. *Journal of Sedimentary Petrology* **35**, 448–53.

KAPLAN, I. R. & RITTENBERG, S. C. 1964. Microbiological fractionation of sulphur isotopes. *Journal of General Microbiology* **34**, 195–212.

KASTEN, S. & JØRGENSEN, B. B. 2000. Sulfate reduction in marine sediments. In *Marine Geochemistry* (eds H. Schulz & M. Zabel), pp. 263–81. Heidelberg: Springer.

KHALAF, F. I. 1990. Occurrence of phreatic dolocrete within Tertiary clastic deposits of Kuwait, Arabian Gulf. *Sedimentary Geology* **68**, 223–39.

KRIJGSMAN, W., GARCÉS, M., AGUSTI, J., RAFFI, I., TABERNER, C. & ZACHARIASSE, W. J. 2000. The 'Tortonian salinity crisis' of the eastern Betics (Spain). *Earth and Planetary Science Letters* **181**, 497–511.

KU, T. C. W., WALTER, L. M., COLEMAN, M. L., BLAKE, R. E. & MARTINI, A. M. 1999. Coupling between sulfur recycling and syndepositional carbonate dissolution: evidence from oxygen and sulfur isotope composition of pore water sulfate, South Florida platform, U.S.A. *Geochimica et Cosmochimica Acta* **63**, 2529–46.

LALOU, C. 1957. Studies on bacterial precipitation of carbonates in sea water. *Journal of Sedimentary Petrology* **27**, 190–5.

LAND, L. S. 1998. Failure to precipitate dolomite at 25°C from dilute solution despite 1000-fold oversaturation after 32 years. *Aquatic Geochemistry* **4**, 361–8.

LEE, C., MCKENZIE, J. A. & STURM, M. 1987. Carbon isotope fractionation and changes in flux and composition of particulate matter resulting from biological activity during a sediment trap experiment in lake Greifen, Switzerland. *Limnology and Oceanography* **32**, 83–96.

LUMSDEN, D. N. 1979. Discrepancy between thin-section and x-ray estimates of dolomite in limestones. *Journal of Sedimentary Petrology* **49**, 429–36.

MACHEL, H. G. 1992. Low-temperature and high-temperature origins of elemental sulfur in diagenetic environments. In *Native Sulfur – Developments in Geology and Exploration* (eds G. R. Wessel & B. H. Wimberly), pp. 3–22. Littleton, Colorado: Society for Mining, Metallurgy, and Exploration, Inc.

MCKENZIE, J. 1981. Holocene dolomitization of calcium carbonate sediments from the coastal sabkhas of Abu Dhabi, U.A.E.: a stable isotope study. *Journal of Geology* **89**, 185–98.

MCKENZIE, J. 1985. Carbon isotopes and productivity in the lacustrine and marine environment. In *Chemical Processes in Lakes. Environmental science and technology* (ed. W. Stumm), pp. 99–118. New York: Wiley.

NAKAI, N. & JENSEN, M. L. 1964. The kinetic isotope effect in the bacterial reduction and oxidation of sulfur. *Geochimica et Cosmochimica Acta* **28**, 1893–912.

NAVARRO HERVÁS, F. & RODRÍGUEZ ESTRELLA, T. 1985. Caracteristicas morfoestructurales de los diapiros Triasicos de Hellín, Ontur, La Celia, Jumilla, La Rosa y Pinoso, en las provincias de Albacete, Murcia y Alicante. *Papeles de Geografica (Fisica)* **10**, 49–69.

ORTÍ, F., ROSELL, L. & ANADÓN, P. 2003. Deep to shallow lacustrine evaporites in the Libros Gypsum (southern Teruel Basin, Miocene, NE Spain): an occurrence of pelletal gypsum rhythmites. *Sedimentology* **50**, 361–86.

ORTÍ, F., ROSELL, L. & ANADÓN, P. 2010. Diagenetic gypsum related to sulfur deposits in evaporites (Libros Gypsum, Miocene, NE Spain). *Sedimentary Geology* **228**, 304–18.

PECKMANN, J., PAUL, J. & THIEL, V. 1999. Bacterially mediated formation of diagenetic aragonite and native sulfur in Zechstein carbonates (Upper Permian, Central Germany). *Sedimentary Geology* **126**, 205–22.

PECKMANN, J. & THIEL, V. 2004. Carbon cycling at ancient methane-seeps. *Chemical Geology* **205**, 443–67.

PIERRE, C. & ROUCHY, J. M. 1988. Carbonate replacements after sulfate evaporites in the middle Miocene of Egypt. *Journal of Sedimentary Research* **58**, 446–56.

PIRLET, H., WEHRMANN, L. M., BRUNNER, B., FRANK, N., DEWANCKELE, J., VAN ROOIJ, D., FOUBERT, A., SWENNEN, R., NAUDTS, L., BOONE, M., CNUDDE, V. & HENRIET, J.-P. 2010. Diagenetic formation of gypsum and dolomite in a cold-water coral mound in the Porcupine Seabight, off Ireland. *Sedimentology* **57**, 786–805.

PLAYÀ, E., ORTÍ, F. & ROSELL, L. 2000. Marine to non-marine sedimentation in the upper Miocene evaporites of the Eastern Betics, SE Spain: sedimentological and geochemical evidence. *Sedimentary Geology* **133**, 135–66.

RICCIONI, R. M., BROCK, P. W. G. & SCHREIBER, B. C. 1996. Evidence for early aragonite in paleo-lacustrine sediments. *Journal of Sedimentary Research* **66**, 1003–10.

ROUCHY, J. M., TABERNER, C., BLANC-VALLERON, M.-M., SPROVIERI, R., RUSSELL, M., PIERRE, C., Di STEFANO, E., PUEYO, J. J., CARUSO, A., DINARÉS-TURELL, J., GOMIS-COLL, E., WOLFF, G. A., CESPUGLIO, G., DITCHFIELD, P., PESTREA, S., COMBOURIEU-NEBOUT, N., SANTISTEBAN, C. & GRIMALT, J. O. 1998. Sedimentary and diagenetic markers of the restriction in a marine basin: the Lorca Basin (SE Spain) during the Messinian. *Sedimentary Geology* **121**, 23–55.

RUCKMICK, J. C., WIMBERLY, B. H. & EDWARDS, A. F. 1979. Classification and genesis of biogenic sulfur deposits. *Economic Geology* **74**, 469–74.

SÁNCHEZ-ROMÁN, M., MCKENZIE, J. A., DE LUCA REBELLO WAGENER, A., RIVADENEYRA, M. A. & VASCONCELOS, C. 2009. Presence of sulfate does not inhibit low-temperature dolomite formation. *Earth and Planetary Science Letters* **285**, 131–9.

SANZ DE GALDEANO, C. 1990. Geologic evolution of the Betic Cordilleras in the Western Mediterranean, Miocene to the present. *Tectonophysics* **172**, 107–19.

SANZ-MONTERO, M. E., RODRÍGUEZ-ARANDA, J. P. & GARCÍA DEL CURA, M. A. 2009. Bioinduced precipitation of barite and celestite in dolomite microbialites. Examples from Miocene lacustrine sequences in the Madrid and Duero Basins, Spain. *Sedimentary Geology* **222**, 138–48.

SCHULZ, H. N. 2002. *Thiomargarita namibiensis*: giant microbe holding its breath. *ASM News* **68**, 122–7.

SCHULZ, H. N. & JØRGENSEN, B. B. 2001. Big bacteria. *Annual Review of Microbiology* **55**, 105–37.

SCHULZ, H. N. & SCHULZ, H. D. 2005. Large sulfur bacteria and the formation of phosphorite. *Science* **307**, 416–18.

SERVANT-VILDARY, S., ROUCHY, J. M., PIERRE, C. & FOUCAULT, A. 1990. Marine and continental water contributions to a hypersaline basin using diatom ecology, sedimentology and stable isotopes: an example in the Late Miocene of the Mediterranean (Hellin Basin, southern Spain). *Palaeogeography, Palaeoclimatology, Palaeoecology* **79**, 189–204.

SHARMA, T. & CLAYTON, R. N. 1965. Measurement of O^{18}/O^{16} ratios of total oxygen of carbonates. *Geochimica et Cosmochimica Acta* **29**, 1347–53.

SLAUGHTER, M. & HILL, R. J. 1991. The influence of organic matter in organogenic dolomitization. *Journal of Sedimentary Petrology* **61**, 296–303.

SMITH, B. N. & EPSTEIN, S. 1971. Two categories of $^{13}C/^{12}C$ ratios for higher plants. *Plant Physiology* **47**, 380–4.

STABEL, H. H. 1986. Calcite precipitation in Lake Constance: chemical equilibrium, sedimentation, and nucleation by algae. *Limnology and Oceanography* **31**, 1081–94.

TALBOT, M. R. 1990. A review of the palaeohydrological interpretation of carbon and oxygen isotopic ratios in primary lacustrine carbonates. *Chemical Geology* **80**, 261–79.

TALBOT, M. R. & KELTS, K. 1990. Paleolimnological signatures from carbon and oxygen isotopic ratios in carbonates from organic carbon-rich lacustrine sediments. In *Lacustrine Basin Exploration – Case studies and modern analogs* (ed. B. J. Katz), pp. 99–112. Tulsa: American Association of Petroleum Geologists Memoir.

TAYLOR, B. E. & WHEELER, M. C. 1984. Stable isotope geochemistry of acid mine drainage: experimental oxidation of pyrite. *Geochimica et Cosmochimica Acta* **48**, 2669–78.

TENZER, G., MEYERS, P. A. & KNOOP, P. 1997. Sources and distribution of organic and carbonate carbon in surface sediments of Pyramid Lake, Nevada. *Journal of Sedimentary Research* **67**, 884–90.

THODE, H. G. & MONSTER, J. 1973 (reprint of 1965). Sulfur-isotope geochemistry of petroleum, evaporites, and ancient seas. In *Marine Evaporites: Origin, diagenesis and geochemistry. Benchmark Papers in Geology* (eds D. W. Kirkland & R. Evans), pp. 363–73. Stroudsburg, Pennsylvania: Dowden, Hutchinson & Ross, Inc.

UTRILLA, R., PIERRE, C., ORTÍ, F. & PUEYO, J. J. 1992. Oxygen and sulphur isotope compositions as indicators of the origin of Mesozoic and Cenozoic evaporites from Spain. *Chemical Geology* **102**, 229–44.

VAN DAM, J. A. & WELTJE, G. J. 1999. Reconstruction of the Late Miocene climate of Spain using rodent palaeocommunity successions: an application of end-member modelling. *Palaeogeography, Palaeoclimatology, Palaeoecology* **151**, 267–305.

VAN LITH, Y., WARTHMANN, R., VASCONCELOS, C. & MCKENZIE, J. 2003. Sulphate reducing bacteria induce low-temperature Ca-dolomite and high Mg-calcite formation. *Geobiology* **1**, 71–9.

VASCONCELOS, C. & MCKENZIE, J. A. 1997. Microbial mediation of modern dolomite precipitation and diagenesis under anoxic conditions (Lagoa Vermelha, Rio de Janeiro, Brazil). *Journal of Sedimentary Research* **67**, 378–90.

VASCONCELOS, C., MCKENZIE, J., BERNASCONI, S. M., CRUJIC, D. & TIEN, A. J. 1995. Microbial mediation as possible mechanism for natural dolomite formation at low temperatures. *Nature* **377**, 220–2.

VASCONCELOS, C., MCKENZIE, J. A., WARTHMANN, R. & BERNASCONI, S. M. 2005. Calibration of the $\delta^{18}O$ paleothermometer for dolomite precipitated in microbial cultures and natural environments. *Geology* **33**, 317–20.

WALTER, L. M., BISCHOF, S. A., PATTERSON, W. P. & LYONS, T. W. 1993. Dissolution and recrystallization in modern shelf carbonates: evidence from pore water and solid phase chemistry. *Philosophical Transactions of the Royal Society of London Series A–Mathematical Physical and Engineering Sciences* **344**, 27–36.

WARREN, J. 2000. Dolomite: occurrence, evolution and economically important associations. *Earth-Science Reviews* **52**, 1–81.

WEAVER, C. E. & BECK, K. C. 1971. *Clay Water Diagenesis During Burial: How mud becomes gneiss*. Geological Society of America, Special Paper 134. Boulder: Geological Society of America, 96 pp.

WRIGHT, D. T. 1999. The role of sulphate-reducing bacteria and cyanobacteria in dolomite formation in distal ephemeral lakes of the Coorong region, South Australia. *Sedimentary Geology* **126**, 147–57.

WRIGHT, D. T. & WACEY, D. 2005. Precipitation of dolomite using sulphate-reducing bacteria from the Coorong Region, South Australia: significance and implications. *Sedimentology* **52**, 987–1008.

YOUSSEF, E. S. A. A. 1989. Geology and genesis of sulfur deposits at Ras Gemsa area, Red Sea coast, Egypt. *Geology* **17**, 797–801.

ZIEGENBALG, S. B., BRUNNER, B., ROUCHY, J. M., BIRGEL, D., PIERRE, C., BÖTTCHER, M. E., CARUSO, A., IMMENHAUSER, A. & PECKMANN, J. 2010. Formation of secondary carbonates and native sulphur in sulphate-rich Messinian strata, Sicily. *Sedimentary Geology* **227**, 37–50.

https://doi.org/10.1017/S0016756811000124 Published online by Cambridge University Press